MNRAS 000, 000–000 (0000) Preprint 27 June 2023 Compiled using MNRAS LaTeX style file v3.0

On the Hα faintness of the North Polar Spur

Yoshiaki SOFUE[1*], Jun KATAOKA[2] and Ryoji IWASHITA[2]
1. Institute of Astronomy, The University of Tokyo, Mitaka, Tokyo 181-0015, Japan
2. Faculty of Science and Engineering, Waseda University, Shinjyuku, Tokyo, 169-8555, Japan

27 June 2023

ABSTRACT

The ratio of the Hα and radio continuum intensities in the North Polar Spur (NPS) is measured to be $\lesssim 50$, two orders of magnitude smaller than the values observed in the typical shell-type old supernova remnants (SNRs), Cygnus Loop and S147, of $\sim 10^4$. The extremely low Hα-to-radio intensity ratio favours the GC explosion model, which postulates a giant shock wave in the hot and low-density Galactic halo with low hydrogen recombination rate, over the local supernova(e) remnant model.

Key words: ISM: individual objects: (North Polar Spur) – ISM: shock waves – ISM: bubbles – Galaxy: centre – galaxies: individual: objects (the Milky Way)

1 INTRODUCTION

The North Polar Spur (NPS) forms the northeastern edge of the giant Galactic bubble, composing the Loop I of radio continuum (Haslam et al. 1982) and X-ray emissions (Snowden et al. 1997; Predehl et al. 2020) with the brightest ridge at $(l, b) \sim (30^\circ, 20^\circ)$ (Sofue & Reich 1979). Due to the sharp-edged shell-like morphology, the NPS is interpreted as a spherical shock wave driven by an explosive energy release at the loop centre.

There are two ideas to explain the origin of the explosion. One is the explosion(s) of nearby supernova(e) (Hanbury Brown et al. 1960; Berkhuijsen et al. 1971; Egger & Aschenbach 1995; Aschenbach & Leahy 1999; Wolleben 2007; Dickinson 2018) in the Sco-Cen OB Associations at a distance of ~ 140 pc (de Zeeuw et al. 1999). This hypothesis assumes supernova remnant(s) expanding in the low temperature, high density ISM at $kT \sim 0.01 - 1$ eV ($T \sim 10^2 - 10^4$ K), $n \sim 1$ H cm^{-3}, and height $|z| \lesssim 30$ pc inside the Galactic disc. However, when most of nearby shell-type SNRs with angular diameters $\gtrsim 1^\circ$ were optically identified by red (Hα)-sensitive emulsions (van den Bergh et al. 1973), the absence of Hα counterpart to NPS, if it is the closest SNR(s), has been a mystery for over half a century (Sofue et al. 1974). In fact, this problem was already pointed out in the earliest paper which suggested the SNR idea for the first time (Hanbury Brown et al. 1960).

The other idea is an explosion in the Galactic nucleus or a starburst in the Galactic Centre (GC) (Sofue 1977; Sofue et al. 2016; Kataoka et al. 2018), which postulates a shock wave propagating in the hot, low-density halo with $kT \sim 0.2$ keV ($\sim 10^{6.3}$ K) and $n \sim 10^{-3}$ H cm^{-3} at $z \sim 3 - 8$ kpc. Because of the high temperature the gas is almost perfectly ionized and the hydrogen recombination is limited, so that the Hα absence may not contradict this idea.

In the present paper, we revisit this classical issue of NPS's optical dimness, which appears to have not been explored by quantitative analysis based on the observational data. We examine the ratio of Hα to radio continuum intensities in the NPS and the most typical shell-type SNRs, Cygnus Loop and S147 (van den Bergh et al. 1973), and focus on the difference in the radiation processes in the shock fronts expanding into the Galactic disc and into the halo.

2 OPTICAL VS RADIO CONTINUUM EMISSIONS

2.1 Data and measured quantities

The radio continuum data were taken from the 408 MHz Bonn-Parkes (Haslam et al. 1982), 1420 MHz Stockert-Villa Elisa (Reich et al. 2001) all-sky survey, and 1420 MHz Bonn 100-m Galactic plane survey (Reich et al. 1990; Reich et al. 1997). Also, radio surveys at 22 (Roger et al. 1999), 150 (Landecker & Wielebinski 1970), 820 (Berkhuijsen 1971), The intensity is measured by the surface brightness $\Sigma = 2kT_{\rm b}/\lambda^2$ in erg cm^{-2} s^{-1} sr^{-1} Hz^{-1}or by brightness temperature $T_{\rm b}$ in K. We also use the integrated intensity $I_{1.4\ {\rm GHz}} = \nu\Sigma$ in unit of erg cm^{-2} s^{-1} sr^{-1} in order to compare with the optical intensity. The Hα data were taken from the Wisconsin Hα all-sky map (WHAM) (Haffner et al. 2003; Haffner et al. 2010), and the intensity unit is Rayleigh (R) defined by

$$1{\rm R} = \frac{10^6}{4\pi}\frac{\rm photons}{\rm cm^2\ s\ sr} = 2.4 \times 10^{-7}\frac{\rm erg}{\rm cm^2\ s\ sr} \quad (1)$$

* E-mail: sofue@ioa.s.u-tokyo.ac.jp

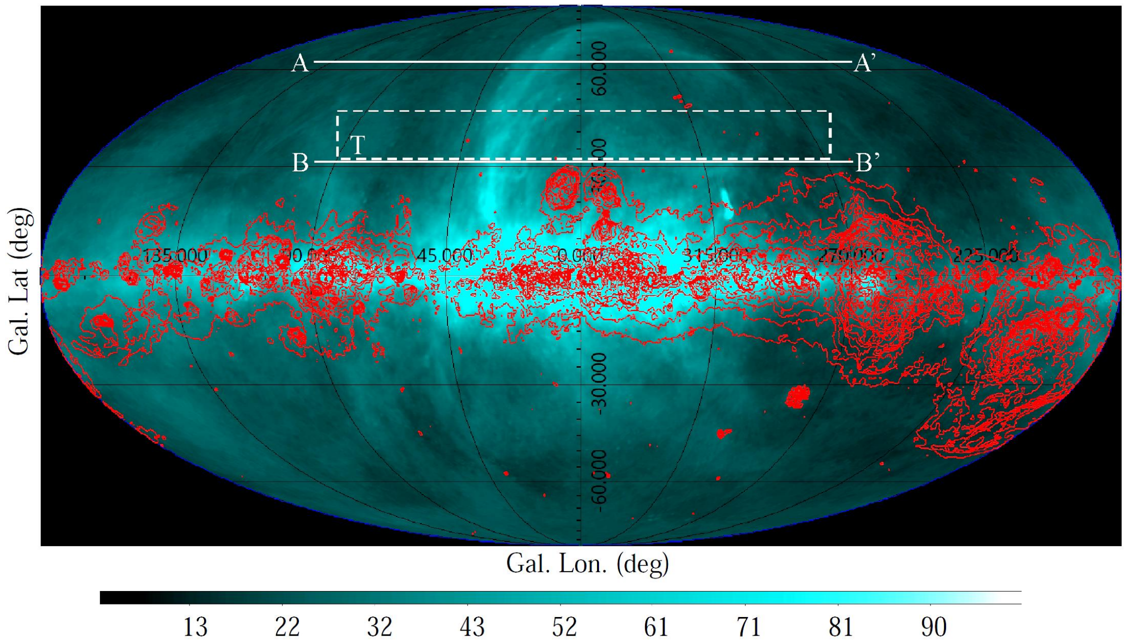

Figure 1. All-sky 408 MHz $T_{\rm b}$ map (in K as bar scaling) (Haslam et al. 1982) overlaid by contours of the Hα intensity at 5, 12, 19, 27, 39, 56R, ... from WHAM survey (Haffner et al. 2003, 2010). Inserted box and lines are used for analyses in Fig. 3 and 4. Angular resolution of the radio map is $0^\circ.85$ and Hα contours are smoothed to $0^\circ.45$. Background filtering is not applied here.

at Hα, and 1 R corresponds to emission measure of EM $=$ 2.25 cm^{-6} pc for gas at a temperature of 8000 K (Haffner et al. 2003).

As we are interested in the Hα-to-radio continuum intensity ratio, we introduce a parameter, $\mathcal{Q}$, defined by

$$\mathcal{Q} = I_{\rm H\alpha}/I_{1.4\ \rm GHz}. \tag{2}$$

Here, $T_{\rm b} = 1$ K corresponds to $I_{1.4\ \rm GHz} = 8.76 \times 10^{-10}$ erg cm^{-2} s^{-1} sr^{-1}. So, a region with $I_{\rm H\alpha} = 1$ R and $T_{\rm b} = 1$ K has the intensity ratio of $\mathcal{Q} = 274$.

2.2 All-sky maps

Figure 1 shows the all-sky radio brightness ($T_{\rm b}$) map at 408 MHz in the (l, b) coordinates obtained from the Bonn-Parkes survey (Haslam et al. 1982) overlaid with contours of the Hα intensity ($I_{\rm H\alpha}$) map from the WHAM survey (Haffner et al. 2003). The FWHM resolution of the 408 MHz map is $0^\circ.85$. The Hα data had a resolution of $6'$, while the contours here are drawn after smoothing to the same resolution as radio. We immediately notice that Loop I, including NPS, is invisible or very weak in Hα despite of the high radio brightness even toward the most prominent ridge at $l \sim 30^\circ$ and $b \sim 20 - 70^\circ$.

2.3 Perpendicular optical filaments in the Aquila Rift

Figure 2 enlarges the radio map at 1420 MHz (Reich et al. 2001) around the brightest region of the NPS by contours superposed on the Hα intensity map. The figure shows several Hα filaments running parallel to the Aquila Rift, which is the dark absorption belt from $(35^\circ, 0^\circ)$ to $(20^\circ, 13^\circ)$, with $I_{\rm H\alpha} \sim 2 - 5$ R at position angle of $PA \sim 120^\circ$, but they cross the NPS at right angle. The perpendicular orientation indicates that these Hα filaments are not related to NPS. We also stress that the darkest part of the Rift at $(l, b) \sim (27^\circ, 8^\circ)$ shows no enhancement across NPS as shown by a comparison of the cross sections of radio and Hα intensities in the lower panel of Fig. 2. This means that no Hα feature associated with NPS exists in front of the Aquila Rift whose distance is ~ 430 pc (Sofue 2015; Sofue & Nakanishi 2017), which contradicts the local origin model for Loop I. However, it does not necessarily deny the possibility that there is Hα associated with NPS, if it is located behind the Rift. In either case, it is difficult to determine how much of the Hα feature is associated with the NPS. We therefore exclude this region from quantitative measurements, and restrict our analysis to the spur at higher latitudes than $b \sim 30^\circ$.

2.4 Intensity profiles

Fig. 3 shows horizontal cross sections of the 408 MHz radio brightness and Hα intensity across the NPS and NPS West, or across the Loop I, at $b = 61^\circ$ and 30° along lines AA' and BB' in Fig. 1, respectively. The radio profiles exhibit a typical double-horn structure indicative of the intensity variation across a spherical shocked shell. On the other hand, the Hα intensity distribution is almost flat except for the broad enhancements by local HII regions ($l \sim -25^\circ$ at $b = 61^\circ$ and $l \sim 0^\circ$ at $b = 30^\circ$), which are unrelated to the NPS.

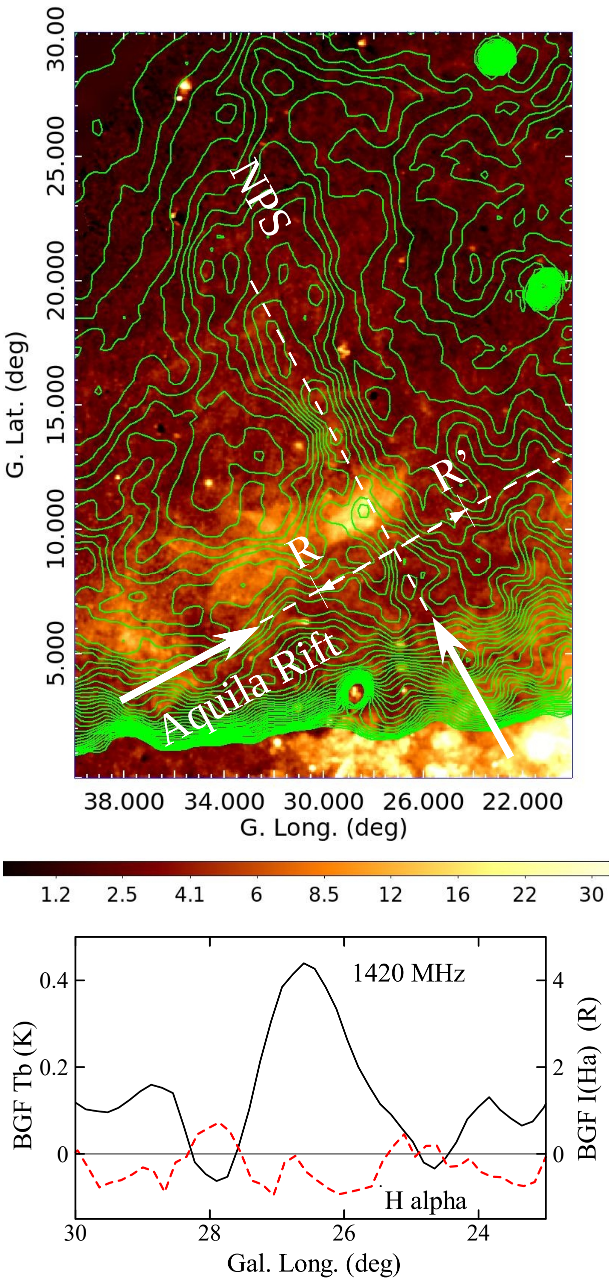

Figure 2. [Top] The brightest ridge of NPS at 1420 MHz by contours (interval 0.1 K; maximum contour $T_\mathrm{b} = 8$ K) from the Stockert survey (Reich et al. 2001) overlaid on the Hα map (scale is non linear by the bar). Many Hα filaments run parallel to the Aquila Rift ($PA \sim 120°$), but they are perpendicular to the NPS ($PA \sim 30°$). No background subtraction is applied in this figure. [Bottom] Cross section of 21-cm and Hα along line R-R'. Here, the smooth emission has been removed by the background-filtering (BGF) technique (Sofue and Reich 1979). (See section 3.2 for the description of BGF)

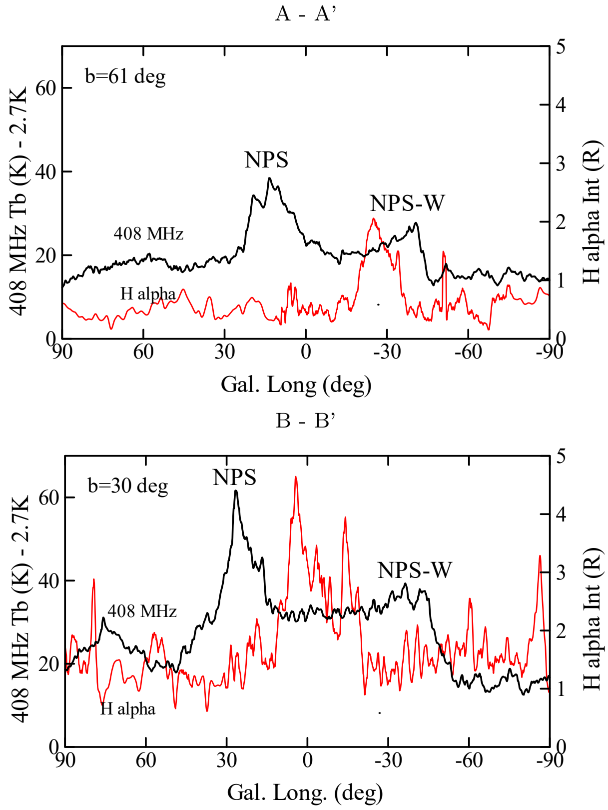

Figure 3. Horizontal cross sections of the 408 MHz radio continuum (black line) and Hα (thin red line) along the lines A-A' and B-B' in Fig. 1 at $b = 30°$ and $61°$. Note the lack of Hα emission corresponding to the radio peaks of NPS and NPS-west. Note that Hα enhancements around $l \sim -30°$ along A-A' and $l \sim 0°$ along B-B' are foreground or background diffuse HII regions not related to the NPS.

2.5 Intensity-intensity plots

The faintness of Hα emission in NPS can be more quantitatively displayed by plotting the Hα intensity against radio intensity in and around the objects using the so-called *TT* plots. Fig. 4 shows Hα intensity in the squared area 'T' of Fig. 1 across the NPS-E (east) and NPS-W (west) plotted against 408 MHz T_b after subtracting the 2.7 K cosmic background emission. Open circles are running means around individual centres of the T_b bins with the bars indicating the dispersion in Hα intensity.

The mean Hα intensity in the OFF NPS region with $T_\mathrm{b} \lesssim 35$ K is measured to be $I_{\mathrm{H}\alpha} \sim 1.22$ R, representing the mean Galactic emission (Haffner et al. 2003) as indicated by the left side arrow marking the region in Fig. 4. The NPS shows up as the high-T_b extension at $35 - 60$ K in the ON-NPS region marked by the right side arrow. So, we here define the NPS in this plot as the area with $T_\mathrm{b}(408\mathrm{MHz}) \gtrsim 35$ K, or $T_\mathrm{b}(1420\mathrm{MHz}) \gtrsim 1$ K for spectral index of $\beta = -2.7$. We, then, measure the mean Hα intensity in this ON-NPS region to be $I_{\mathrm{H}\alpha} \sim 1.3$ R. Although the excess of ON-NPS $I_{\mathrm{H}\alpha}$ over OFF-NPS value is ~ 0.1 R, we here estimate the excess to be $\Delta I_{\mathrm{H}\alpha} \sim 0.2$R, considering the scatter and dispersion of the plotted values. This yields the Hα-to-radio intensity ratio of $\mathcal{Q} \lesssim 50$ at 1.4 GHz.

The Hα intensity yields the upper limit to the emission measure as EM $\lesssim 0.5$ cm^{-6} pc for assumed electron temperature $T_\mathrm{e} = 10^4$ K. The values may be compared with those estimated for the SNR, Cygnus Loop, where $T_\mathrm{b} \sim 1$ K and $I_{\mathrm{H}\alpha} \sim 20$ R, yielding $\mathcal{Q} \sim 6 \times 10^3$, and EM ~ 50 cm^{-6} pc for

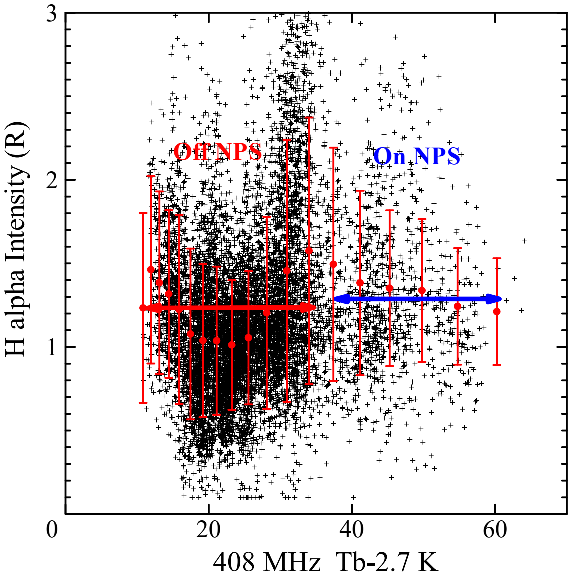

Figure 4. *TT* Plot of the Hα intensity against 408 MHz brightness temperature $T_{\rm b}$ after subtracting 2.73 K in the area 'T' of Fig. 1 (from $l \sim 270^\circ$ to 90° and $b = +30^\circ$ to $+45^\circ$). The blue and red arrows indicate the on-NPS and off-NPS emissions, respectively. The background-filtering is not applied here.

10^4 K as obtained from individual Hα observations (Hester et al. 1986). We list the estimated values in table 1.

3 COMPARISON WITH SNRS

3.1 Maps

Fig. 5 shows overlays of radio continuum brightness at 1420 MHz of the Cygnus Loop and S147 on Hα intensity maps, where the radio maps were taken from the Bonn-100m Galactic plane survey (Reich et al. 1990; Reich et al. 1997). The SNRs are visible both in radio and Hα emissions. Such Hα-radio association is often observed in Galactic radio SNRs (Uyanıker et al. 2004; Xiao et al. 2008), and seems also to happen in the spiral galaxy M31 (Braun & Walterbos 1993). On the other hand, Hα is hardly visible in the NPS despite of the clear and sharp radio ridge as shown in Figs 1 and 2. The NPS is, thus, extraordinarily fainter in Hα compared with the usual SNRs.

3.2 Spectra (SED)

Fig. 6 shows variation of peak intensities at various frequencies along the NPS ridge as obtained using background-filtered (BGF) maps (Sofue & Reich 1979) of the radio and Hα sky surveys. The BGF subtracts background emission and creates a nearly zero-adjusted intensity distribution of sources with scale sizes greater than a smoothing beam width[1]. We used a box-shaped one-dimensional smoothing beam with full width of 10° in the longitude direction at each latitudinal grid. The one-dimensional smoothing was so chosen that it avoids unnecessary smearing effect by the steep intensity gradient perpendicular to the Galactic disc. Although the angular resolutions are different at different frequencies, the NPS is sufficiently resolved, and we used the peak intensities read on the thus obtained BGF maps for the spectral analysis in this section.

[1] The 'background' is defined as a smoothed map after iterative clipping of peaky sources, so that it traces the valleys of the intensity distribution.

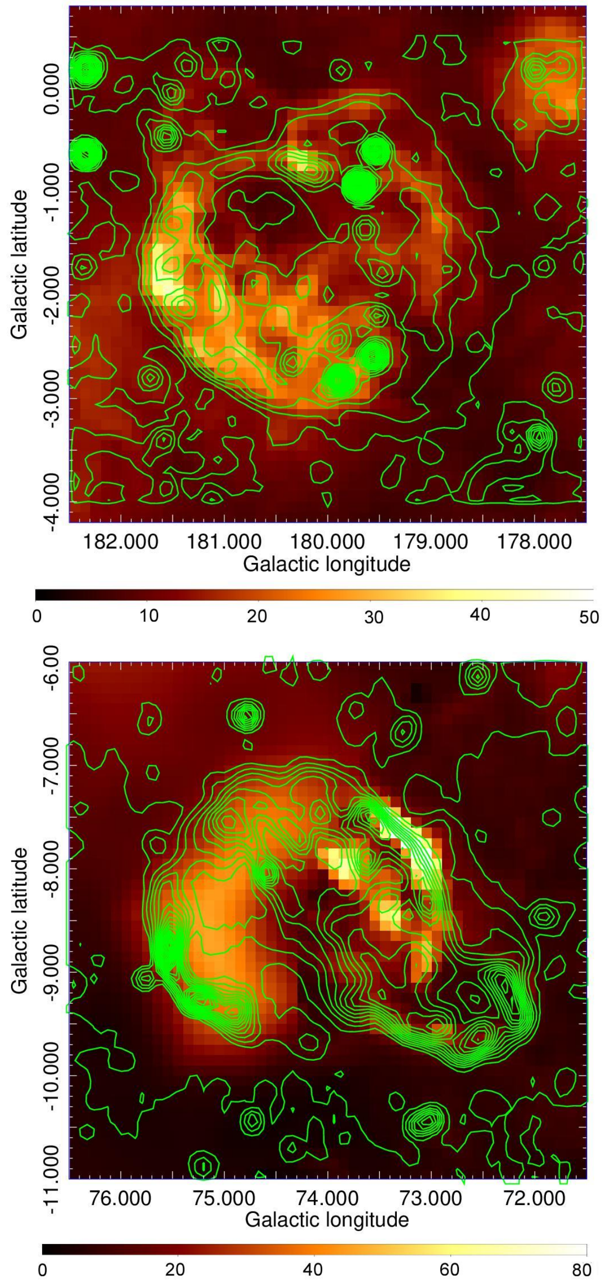

Figure 5. 1420 MHz maps of SNRs (top: S147, bottom: Cygnus Loop) from the Bonn-100 m Galactic plane survey (Reich et al. 1990, 1997) by contours at an interval of 0.1 K overlaid on Hα intensity maps from 0 to 50R for S147 and 0 to 80R for Cygnus Loop as indicated by the bars. Compare these maps with Figs. 1 and 2, where NPS is not visible in Hα despite of the much lower intensity levels.

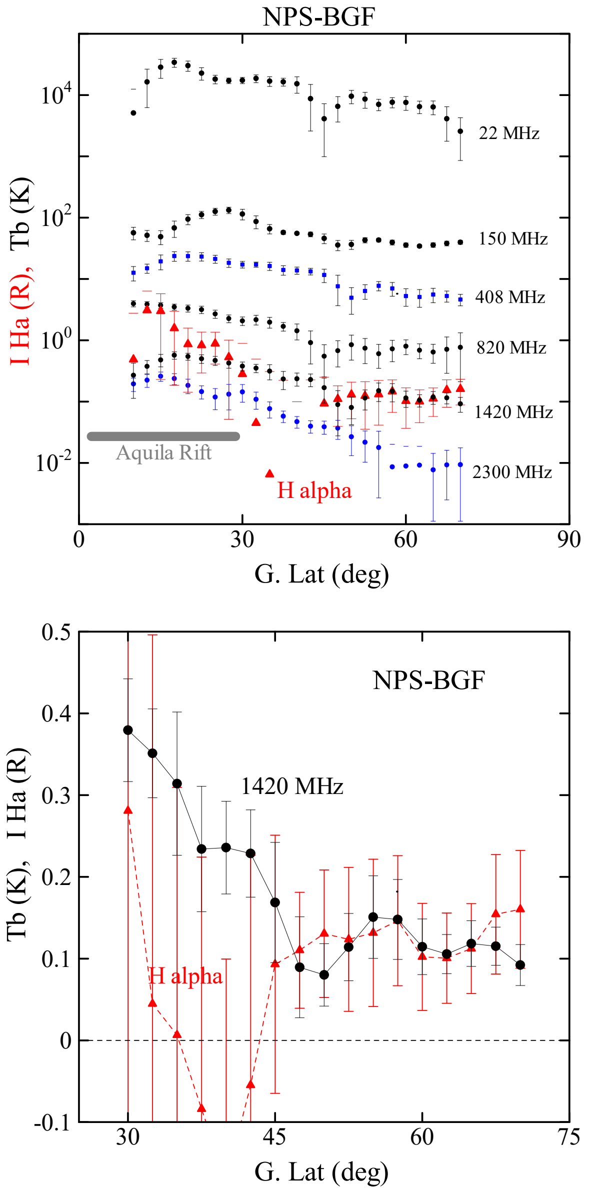

Figure 6. [Top] Intensity profiles along the NPS ridge using the BGF maps at 22 to 2300 MHz and Hα maps taken from the surveys cited in section 2.1. [Bottom] Same, but enlarged for 1420 MHz and Hα profiles.

Fig. 7 shows a spectral energy distribution (SED) of the NPS at $b = 30°$, $45°$ and $60°$ as obtained from the intensity plot along the NPS ridge shown in Fig. 6. We also plot SEDs of the northern shell edge of Cygnus Loop and eastern edge of S147. The background emissions around SNRs are subtracted by measuring averaged brightness in a small area without significant emission features about half a shell radius outside each shell edge at the same Galactic latitude. The Hα extinction has been corrected by $A_{\mathrm{H}\alpha} = 0.2$ and 0.6 mag., respectively, for Cygnus Loop and S147, as described in section 3.4. However, the correction is not applied to the NPS, because we here compare the spectra, when they are assumed to be the same type (SNR-type) objects, and so

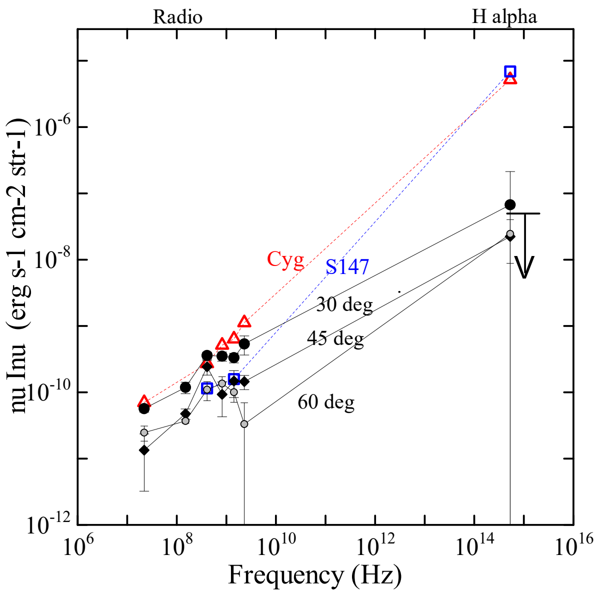

Figure 7. Spectral energy distributions (SED) of the NPS at $b = 30°$ (dots), $45°$ (diamonds), and $60°$ (grey circles) made from the peak-intensity profiles in Fig. 6. Intensities of the northern shell edge of the Cygnus Loop (red triangles) and eastern shell edge of S147 (blue squares) are also plotted. Interstellar extinction of Hα is corrected for according to their distances, while no correction is made for NPS here for its assumed distance of 140 pc in this diagram. The arrow indicates the estimated upper limit of $I_{\mathrm{H}\alpha}$ from the TT analysis.

the NPS is assumed to be located at a distance of ~ 140 pc with negligible extinction.

The radio spectra of NPS and SNRs are consistent with those from more accurate analyses (Iwashita et al. 2023; Xiao et al. 2008; Uyanıker et al. 2004), and show that the radio intensities of the NPS and SNRs are comparable. However, a significant difference is found at Hα, where the NPS is fainter than SNRs by two orders of magnitude. The upper limit to the Hα intensity of the NPS as obtained from the TT analysis is indicated by the arrow.

3.3 TT

In Fig. 8 we display TT plots in linear and logarithmic scaling for the SNRs shown in Fig. 5 in comparison with that of the NPS in region T of Fig. 1. The lowest values of Hα and radio intensities in each TT plot representing the background emission are subtracted. The plots for the SNRs indicate that the Hα intensity is well correlated with the radio intensity by a relation $I_{\mathrm{H}\alpha} \propto T_{\mathrm{b}}$. Using the gradient of the linear plot in the upper panel we obtain the Hα-to-radio intensity ratio of $\mathcal{Q} \sim 1.1 \times 10^4$ both for Cygnus Loop and S147. On the other hand, the NPS's plot shows no clear correlation between Hα and radio intensities.

3.4 Interstellar extinction

The radio continuum emissions are absorption free in the circumstances discussed here regardless of the distance. In the SNR hypothesis, which assumes a distance to NPS less

Table 1. Intensities of the NPS and SNR Cygnus Loop

Object	Quantity		EM (cm^{-6} pc)	T_e(K)	Remark
NPS	X ray (3/4 keV)	$I_\mathrm{X} \sim 2 \times 10^{-4}$ cts/s/amin^2	EM ~ 0.1	$T_\mathrm{e} \sim 10^{6.5}$ (0.3 keV)	1, 2, 3
	Hα for X-ray EM	$I_{\mathrm{H}\alpha} \sim 4 \times 10^{-5}$ R	ibid (~ 0.1)	for $10^{6.5}$ K	
	Hα observed here	$I_{\mathrm{H}\alpha} \lesssim 0.2$ R	EM $\lesssim 1.4 \times 10^2$	for 10^6 K	
	Hα observed here	$I_{\mathrm{H}\alpha} \lesssim 0.2$ R	EM $\lesssim 0.4$	for 10^4 K	
	Radio 1.42 GHz	$T_\mathrm{b} \sim 1$ K			
	Hα/radio intensity ratio	$\mathcal{Q} \lesssim 50$			
Cygnus Loop	Xray (3/4 keV)	$I_\mathrm{X} \sim 10^{-2}$ cts/s/amin^2	EM ~ 1	$T_\mathrm{e} \sim 6 \times 10^6$ (0.5 keV)	4
	Hα	$I_{\mathrm{H}\alpha} \sim 20 - 40$ R	EM ~ 50	for 10^4 K	5
	Radio 1.42 GHz	$T_\mathrm{b} \sim 1$ K			
	Hα/radio intensity ratio	$\mathcal{Q} \sim 1.1 \times 10^4$			Fig. 8.

1. X-ray intensity was read from ROSAT all-sky map at 3/4 keV (R4 band) (Snowden et al. 1997) (1 cts/s/arcmin^2 = 400 Jy sr^{-1} = 9.6×10^{-4} erg cm^{-2} s^{-1} keV^{-1}); 2,3:(Kataoka et al. 2013; Yamamoto et al. 2022); 4. (Uchida et al. 2008); 5.(Hester et al. 1986).

than ~ 140 pc, the interstellar dust extinction of the Hα emission is negligible in the entire Loop I even at low or zero latitudes, because it is located in front of the Aquila Rift at a distance of ~ 0.4 kpc (Sofue 2015; Sofue & Nakanishi 2017). This assumption is used in the figures where NPS and SNRs are compared.

The SNR Cygnus Loop is observed to have $A_v = 0.25$ mag, or $A_{\mathrm{H}\alpha} \sim 0.2$ (Fesen et al. 2018). S147 has foreground extinction of $A_v = 0.7$ mag ($A_{\mathrm{H}\alpha} \sim A_r \sim 0.6$) (Fesen et al. 1985), and $A_v \sim 1.2$ mag or $A_r \sim 0.9$ including the internal extinction (Chen et al. 2017). Therefore, the Hα intensities observed toward Cygnus Loop and S147 in Fig. 5 and 8 are under-estimated by about factors of 1.2 and 1.7, respectively. These factors for the SNRs are corrected in Fig. 7 in order to compare with NPS as a local object with negligible extinction.

In the GC explosion hypothesis of NPS, which assumes a distance of ~ 8 kpc, the optical (visual) extinction can be estimated by the general law relating it to HI column density, N_HI, by

$$A_v = N_\mathrm{HI}/1.79 \times 10^{21} \mathrm{HI\ cm}^{-2} \quad (3)$$

(Predehl & Schmitt 1995). Measuring the HI column density from the all-sky integrated HI intensity map (Kalberla et al. 2007), we obtain $N_\mathrm{HI} \sim 1.1 \times 10^{21}$ H cm^{-2} at $b \sim 15^\circ$, $\sim 0.7 \times 10^{21}$ at 30°, and $\sim 0.15 \times 10^{21}$ at $\sim 60^\circ$. Then, assuming (Gordon et al. 2003)

$$A_{\mathrm{H}\alpha} \simeq A_\mathrm{r} = 0.8 A_v, \quad (4)$$

we obtain $A_{\mathrm{H}\alpha} \sim 0.49$, 0.31 and ~ 0.07 mag. at $b \sim 15^\circ$, 30°, and 60°, respectively. Or, the Hα intensities are under-estimated by a factor of 1.6, 1.3 and 1.07, respectively, at these latitudes. The region closer to the low galactic latitudes of NPS suffers from heavier extinction by the dust lane of the Aquila Rift, where we cannot give a conclusive discussion.

4 SUMMARY AND DISCUSSION

4.1 Summary

Analysis has shown that the Hα-to-1.4 GHz radio intensity ratio for NPS ($\mathcal{Q} \lesssim 50$) is more than two orders of magnitude smaller than that for typical shell-type SNRs, Cygnus Loop and S147 ($\mathcal{Q} \sim 1.1 \times 10^4$). No evidence of H$\alpha$ association was found along NPS, even towards the brightest and sharpest ridge at $b \sim 8 - 20^\circ$. The low Hα intensity favours the GC explosion model over the local supernova explosion model.

Below we discuss the implication of the results for the two models about the origin of NPS. In either model of local or GC origin, it should be noted that NPS is much larger in size than the other known SNRs or bubbles. This may lead to various differences in environments and physical conditions where the NPS is situated. The $\mathcal{Q}$ value would be useful to distinguish such differences from each other regardless of the size and distance.

4.2 On the local bubble model

It is difficult to interpret the Hα-dark NPS as an ordinary supernova remnant such as the Cygnus Loop or S147 that exploded in the dense ($\rho \sim 1$ H cm^{-3}) and cold ($T \lesssim 10^4$ K) Galactic disc, where the hydrogen recombination is high and the shock compressed shells efficiently emit Hα line at $\sim 20 - 40$ R. If NPS is a remnant of multiple supernovae exploded in a local OB association, much stronger shock waves would cause brighter Hα. If it is a similar object to the Orion-Eridanus super bubble (Pon et al. 2016) as seen in Fig. 1 around $(l, b) \sim (200^\circ, -20^\circ)$, it should be as bright as $\sim 10 - 20$ R. If it is associated with high-latitude HI spurs at local velocities (Heiles et al. 1980), then the shocked area in touch with the NPS should emit Hα by the same mechanism as above. Thus, the local origin models have difficulty explaining the Hα faintness of NPS.

4.3 On the GC explosion model

The Hα faintness can be naturally explained by the GC explosion model. The model postulates a shock wave propagating in the Galactic halo at $T \sim 10^{6.3}$ K. The temperature in NPS is observed to be much higher at $\sim 10^{6.5}$ K, while the emission measure is rather small at EM ~ 0.1 cm^{-6} pc (Kataoka et al. 2013; Kataoka et al. 2018; Yamamoto et al. 2022). In such a hot plasma the hydrogen recombination rate is 10^{-2} times that in the ISM at $T \sim 8000$ K, $\alpha(10^{6.5}\mathrm{K}) \sim 10^{-2} \alpha(8000\mathrm{K})$ (Hummer 1994). Knowing that 1 R at this temperature corresponds to 2.25 cm^{-6} pc (Haffner et al. 2003), it leads to $I_{\mathrm{H}\alpha} \sim 10^{-2} EM/2.25 \sim$

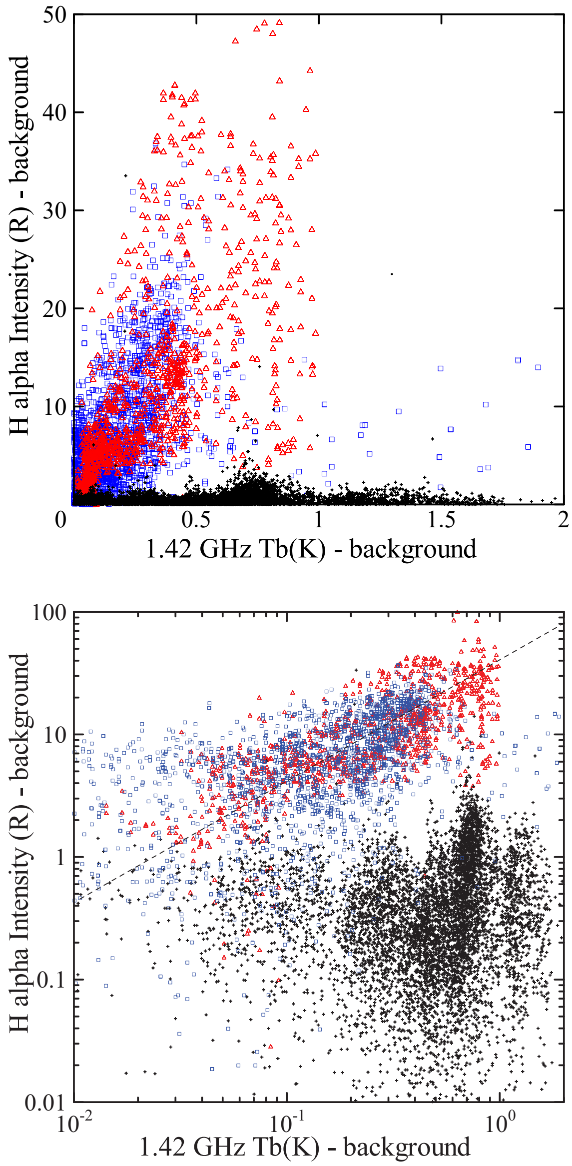

Figure 8. Linear and logarithmic TT plots of Hα against radio intensities for the NPS (black dots) converted to 1.4 GHz compared with those at 1.4 GHz for Cygnus Loop (red triangles) and S147 (blue squares). Approximate base-line (background) intensities in each object's area are subtracted. The dashed line represents the Hα-to-radio intensity ratio of $\mathcal{Q} \sim 1.1 \times 10^4$.

4×10^{-3} R, which is consistently below the observed upper limit of $I_{\rm H\alpha}$(NPS) $\lesssim$ 0.2 R. Thus, the GC bubble model seems plausible to explain the observed Hα faintness of the NPS.

The Hα property of NPS gives further constraint on the GC origin model. A galactic-scale wind such as observed in starburst galaxy NGC 3079 (Cecil et al. 2002) or M82 (Lehnert et al. 1999) presumes a large Hα shell in the halo. However, such an Hα shell is not observed in NPS. So, NPS may be a more spherical bubble directly exposed to the halo's hot plasma. Even so, the root region might emit Hα associated with the 1-kpc conical wind of HI (Sofue 2022; Sofue & Kataoka 2021) and X-ray (Bland-Hawthorn & Cohen 2003), but it is hidden behind the Aquila Rift. In this case the NPS will be a giant bubble similar to that observed in NGC 253, where 1-kpc scale Hα wind blows near the nucleus (Westmoquette et al. 2011) and a giant X-ray and radio bubbles are expanding into the halo (Sofue & Vogler 2001).

ACKNOWLEDGEMENTS

The data analysis was carried out on the computer system at the Astronomy Data Center of the National Astron. Obs. of Japan. The authors are indebted to the groups of the Bonn-Stockert radio (Dr. P. and W. Reich) and WHAM (Dr. L. M. Haffner) surveys for the archival data base. A part of this research was supported by Japan Science and Technology Agency (JST) ERATO Grant Number JPMJER2102 and JSPS Kakenhi Grant Number 20K20923, Japan.

DATA AVAILABILITY

The radio and Hα fits data were downloaded from the URL:
https://lambda.gsfc.nasa.gov/product/foreground/fg_diffuse.html, and
http://www3.mpifr-bonn.mpg.de/survey.html.

CONFLICT OF INTEREST

The authors declare that there is no conflict of interest.

REFERENCES

Aschenbach, B., Leahy, D. A. 1999, A&A, 341, 602

Berkhuijsen, E. M. 1971, A&A, 14, 359

Berkhuijsen, E. M., Haslam, C. G. T., Salter, C. J. 1971, A&A, 14, 252

Bland-Hawthorn, J., Cohen, M. 2003, ApJ, 582, 246

Braun, R., Walterbos, R. A. M. 1993, A&AS, 98, 327

Cecil, G., Bland-Hawthorn, J., Veilleux, S. 2002, ApJ, 576, 745

Chen, B.-Q., Liu, X.-W., Ren, J.-J. et al. 2017, MNRAS, 472, 3924

de Zeeuw, P. T., Hoogerwerf, R., de Bruijne, J. H. J. et al. 1999, AJ, 117, 354

Dickinson, C. 2018, Galaxies, 6, 56.

Egger, R. J., Aschenbach, B. 1995, A&A, 294, L25

Fesen, R. A., Blair, W. P., Kirshner, R. P. 1985, ApJ, 292, 29

Fesen, R. A., Neustadt, J. M. M., Black, C. S. et al. 2018, MNRAS, 475, 3996

Gordon, K. D., Clayton, G. C., Misselt, K. A. et al. 2003, ApJ, 594, 279

Haffner, L. M., Reynolds, R. J., Tufte, S. L. et al. 2003, ApJS, 149, 405

Haffner, L. M., Reynolds, R. J., Madsen, G. J. et al. 2010, The Dynamic Interstellar Medium: A Celebration of the Canadian Galactic Plane Survey, 438, 388 doi:10.48550/arXiv.1008.0612

Hanbury Brown, R., Davies, R. D., Hazard, C. 1960, The Observatory, 80, 191

Haslam, C. G. T., Salter, C. J., Stoffel, H., Wilson, W. E. 1982, AAS, 47, 1

Heiles, C., Chu, Y.-H., Troland, T. H. et al. 1980, ApJ, 242, 533

Hester, J. J., Raymond, J. C., Danielson, G. E. 1986, ApJ, 303, L17

Hummer, D. G. 1994, MNRAS, 268, 109

Iwashita, R., Kataoka, J., Sofue, Y. 2023, submitted to MNRAS.

Jonas, J. L. Baart, E. E. 1995, ApSS, 230, 351
Kalberla P. M. W., Dedes L., Kerp J., Haud U., 2007, A&A, 469, 511
Kataoka, J., Tahara, M., Totani, T. et al. 2013, ApJ, 779, 57
Kataoka J., Sofue Y., Inoue Y., Akita M., Nakashima S., Totani T., 2018, Galax, 6, 27
Kataoka J., Yamamoto, M., Nakamura, Y. et al., 2021, ApJ, 908, 14
Lallement, R., Vergely, J. L., Babusiaux, C. et al. 2022, A&A, 661, A147
Landecker, T. L., Wielebinski, R. 1970, Australian Journal of Physics and Astrophysics Supplement 16, 1
Lehnert, M. D., Heckman, T. M., Weaver, K. A. 1999, ApJ, 523, 575
Pon, A., Ochsendorf, B. B., Alves, J. et al. 2016, ApJ, 827, 42
Predehl, P, Schmitt, J. H. M. M. 1995, A&A, 293, 889
Predehl, P., Sunyaev, R. A., Becker, W. et al. 2020, Nature, 588, 227
Reich, W., Reich, P., Fürst, E. 1990, A&AS, 83, 539
Reich, P., Reich, W., Fürst, E. 1997, A&AS, 126, 413
Reich, P., Testori, J. C., Reich, W. 2001, A&A, 376, 861
Roger, R. S., Costain, C. H., Landecker, T. L. et al. 1999, A&AS, 137, 7
Snowden S. L. et al., 1997, ApJ, 485, 125
Sofue, Y. 1977, AA 60, 327
Sofue, Y. 2015, MNRAS, 447, 3824
Sofue, Y. 2022, PASJ, 74, L23
Sofue Y., Habe A., Kataoka J. et al. 2016, MNRAS, 459, 108
Sofue, Y., Hamajima, K., Fujimoto, M. 1974, PASJ, 26, 399
Sofue, Y., Kataoka, J. 2021, MNRAS, 506, 2170
Sofue, Y ., Nakanishi, H. 2017, MNRAS, 464, 783
Sofue, Y., Reich, W. 1979 AAS 38, 251
Sofue, Y, Vogler, A. 2001, A&A, 370, 53
Uchida, H., Tsunemi, H., Katsuda, S. et al. 2008, ApJ, 688, 1102
Uyanıker, B., Reich, W., Yar, A. et al. 2004, A&A, 426, 909
van den Bergh, S., Marscher, A. P., Terzian, Y. 1973, ApJS, 26, 19
Westmoquette, M. S., Smith, L. J., Gallagher, J. S. 2011, MNRAS, 414, 3719
Wolleben, M. 2007, ApJ, 664, 349
Xiao, L., Fürst, E., Reich, W. et al. 2008, A&A, 482, 783
Yamamoto, M., Kataoka, J., Sofue, Y. 2022, MNRAS, 512, 2034